Island Arc

Island Arc (2014)

Research Article

Gas hydrate saturation at Site C0002, IODP Expeditions 314 and 315, in the Kumano Basin, Nankai trough

Ayumu Miyakawa,[1,*] Saneatsu Saito,[2] Yasuhiro Yamada,[3] Hitoshi Tomaru,[4] Masataka Kinoshita,[5] and Takeshi Tsuji[6]

[1]*Geological Survey of Japan, AIST, AIST Tsukuba Central 7, Higashi-1-1-1, Tsukuba, Ibaraki 305-8567, Japan (email: miyakawa-a@aist.go.jp),* [2]*Institute for Research on Earth Evolution, Japan Agency for Marine-Earth Science and Technology, 2-15 Natsushima-cho, Yokosuka 237-0061, Japan,* [3]*Department of Urban Management, Kyoto University, C1-108 Katsura, Nishikyo-ku, Kyoto 615-8540, Japan,* [4]*Department of Earth Sciences, Chiba University, 1-33, Yayoi-cho, Inage-ku, Chiba 263-8522, Japan,* [5]*Kochi Institute for Core Sample Research, Japan Agency for Marine-Earth Science and Technology, 200 Monobe Otsu, Nankoku City, Kochi 783-8502, Japan and* [6]*International Institute for Carbon-Neutral Energy Research (WPI-I2CNER), Kyushu University, 744 Motooka, Nishi-ku, Fukuoka 819-0395, Japan*

Abstract The degree of gas hydrate saturation at Integrated Ocean Drilling Program (IODP) Site C0002 in the Kumano Basin, Nankai Trough, was estimated from logging-while-drilling logs and core samples obtained during IODP Expeditions 314 and 315. Sediment porosity data necessary for the calculation of saturation were obtained from both core samples and density logs. Two forms of the Archie equation ('quick-look' and 'standard') were used to calculate gas hydrate saturation from two types of electrical resistivity log data (ring resistivity and bit resistivity), and a three-phase Biot-type equation was used to calculate gas hydrate saturation from P-wave velocity log data. The gas hydrate saturation baseline calculated from both resistivity logs ranges from 0% to 35%, and that calculated from the P-wave velocity log ranges from 0% to 30%. High levels of gas hydrate saturation (>60%) are present as spikes in the ring resistivity log and correspond to the presence of gas hydrate concentrations within sandy layers. At several depths, saturation values obtained from P-wave velocity data are lower than those obtained from bit resistivity data; this discrepancy is related to the presence of free gas at these depths. Previous research has suggested that gas from deep levels in the Kumano Basin has migrated up-dip towards the southern and seaward edge of the basin near Site C0002. The high saturation values and presence of free gas at site C0002 suggest that a large gas flux is flowing to the southern and seaward edge of the basin from a deeper and/or more landward part of the Kumano Basin, with the southern edge of the Kumano Basin (the location of site C0002) being the main area of fluid accumulation.

Key words: *Chikyu*, Expedition 314, Expedition 315, free gas, gas hydrate, Integrated Ocean Drilling Program, Kumano forearc basin, logging data analysis, Nankai trough, Site C0002.

INTRODUCTION

Gas hydrates are (i) a potential future energy resource, (ii) a cause of submarine geohazards, and (iii) a key factor in global climate change (Kvenvolden & Keith 1993). Sediments containing methane hydrates are characterized by specific pressure–temperature conditions that occur in regions of permafrost and beneath the sea at outer continental margins (Kvenvolden 1988); for example, gas hydrates are widely distributed in accretionary prisms and overlying forearc basins in subduction zones (Yamada *et al.* 2014),

*Correspondence.

Received 28 June 2013; accepted for publication 14 January 2014.

doi:10.1111/iar.12064

accretionary prisms of the Middle American Trench (Kvenvolden & McDonald 1985), offshore of Costa Rica (Shipboard Scientific Party 1997), and along the Cascadian margin (Tréhu *et al.* 2003; Expedition 311 Scientists 2005). Gas hydrates in subduction margins have also been identified in the Nankai Trough offshore from Japan, based on the presence of bottom-simulating reflectors (BSRs; e.g. Ashi *et al.* 2002; Baba & Yamada 2004). The identification of areas of gas hydrate accumulation and migration of hydrate-forming fluids in accretionary prism and overlying forearc basin sequences is therefore one of the most important areas of research in the subduction zone offshore from Japan. Our aim in this paper is to estimate how much gas hydrate is concentrated, and to reveal the dynamics of free gas that forms gas hydrate, in the Kumano forearc Basin, Nankai Trough.

Previous scientific drilling expeditions have identified the presence of gas hydrates in the Nankai Trough, located to the southwest of the Japan islands. These gas hydrates are located in the toe of an accretionary prism off Muroto (Taira *et al.* 1992) and offshore from the mouth of the Tenryu River (e.g. Tsuji *et al.* 2004). The Nankai Trough accretionary prism and the Kumano forearc Basin have massive gas hydrate in their formations (e.g. Bangs *et al.* 2010; Kinoshita *et al.* 2011). The NanTroSEIZE drilling program of the Integrated Ocean Drilling Program (IODP) undertook investigations across the Nankai Trough accretionary prism and the Kumano forearc Basin, employing the drilling vessel *Chikyu* (e.g. Expedition 314 Scientists 2009a; Expedition 319 Scientists 2010), including drilling into gas hydrate-bearing sediments of the Kumano Basin (Kinoshita *et al.* 2009; Fig. 1).

Recent research conducted as part of the NanTroSEIZE program identified both the source and location of gas for the gas hydrates in the southern or seaward region of the Kumano Basin. Doan *et al.* (2011) determined that free gas is generated by organic-rich layers at IODP Site C0009 (Fig. 1), landward from the edge of the basin, and suggested that this free gas migrates upwards and accumulates within tilted layers of coarser sediments. This is consistent with the characteristics of logging undertaken at the seaward edge of the Kumano Basin at IODP Site C0002 (Saito *et al.* 2010; Fig. 2), although the actual amount of gas hydrate in this area is still unknown. Here, we present new calculations for the saturation of gas hydrate in sediments at the seaward edge of the Kumano Basin at Site C0002; these data reveal fluid migration pathways and fluxes at the edge of the Kumano Basin.

MATERIALS AND METHODS

DATASET

A well-developed BSR has been imaged by seismic data obtained at IODP Site C0002 in the Kumano Basin (Fig. 1). Logging-while-drilling (LWD) logs recorded during Expedition 314 provide comprehensive *in situ* information on the nature of gas hydrate at this site (Expedition 314 Scientists 2009a; Tobin *et al.* 2009; Fig. 2). Four primary logging units were defined in addition to two zones within logging Unit II, and gas-hydrate-bearing zones were defined on the basis of logging data, and labeled Zone A (Table 1; Expedition 314 Scientists 2009a). During Expedition 315, drilling penetrated the uppermost 1400 m of the Kumano Basin sequence, and cores were obtained from both the basin sedimentary sequence and the underlying accretionary prism. However, no core samples were obtained from depths of 200–400 m below the seafloor during either Expedition 314 or 315, which are depths at which gas hydrates are present at this site. The LWD electrical resistivity and P-wave velocity (Vp) logs from Site C0002 indicate the presence of gas hydrate at LWD depths of 218.1–400.4 m below the seafloor (LSF) (Zone A, logging Unit II; Expedition 314 Scientists 2009a).

Here, we focus on calculating the degree of gas hydrate saturation in the Kumano Basin at Site C0002, using data from LWD logs obtained during Expedition 314. These calculations require estimations of some parameters, such as porosity, bulk modulus and shear modulus, using core samples obtained during Expedition 315 from above and below the hydrate-bearing zone. The caliper log from Hole C0002A was used to estimate borehole conditions (Fig. 2A), and the degree of gas hydrate saturation was estimated primarily from logging-derived ring and bit resistivity (Fig. 2B,C, respectively) and Vp data (Fig. 2D). Ring resistivity is a focused lateral resistivity measurement with a vertical resolution of 2–3 inches (5–7.5 cm) and a depth of investigation of 7 inches (17.8 cm; Expedition 314 Scientists 2009b), whereas bit resistivity is the resistivity between the lower portion of the logging tool and the drilling bit, with a vertical resolution of 12–24 inches (30.5–61.1 cm)

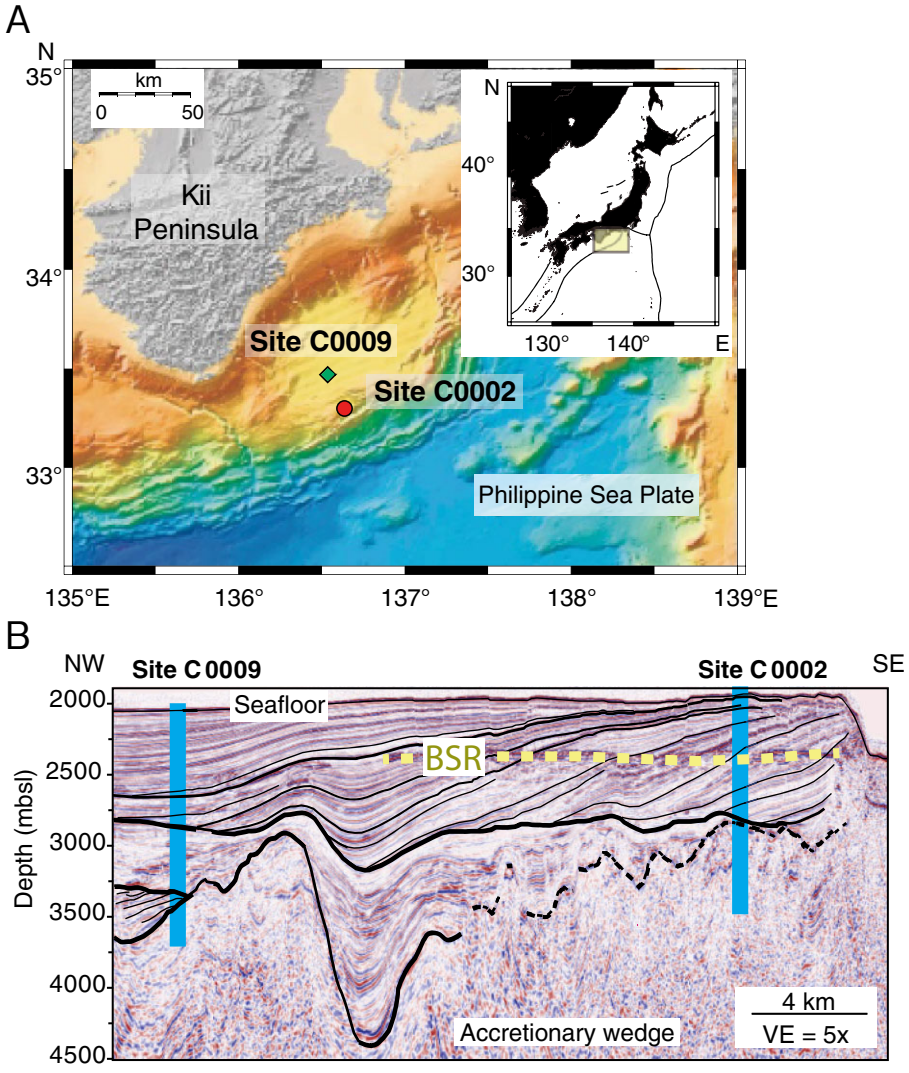

Fig. 1 The locations of NanTroSEIZE Sites C0002 and C0009 (modified after Expedition 319 Scientists 2010). (A) Location of IODP Expedition 314 and 315 in the Kumano Basin. Site C0002 is marked by a red dot, and the location of Site C0009 is marked by a green square. The inset map on the upper right indicates a plate-tectonic framework of the Japanese islands and locations of IODP Expedition 314 and 315 sites (rectangle). (B) The locations of Site C0002 and Site C0009 within a seismic profile across the Kumano Basin offshore from the Kii Peninsula. The dashed yellow line is the location of bottom-simulating reflectors (BSR). VE, vertical exaggeration.

and a depth of investigation of 12 inches (30.5 cm; Expedition 314 Scientists 2009b). The Vp values are the inverse of the measured compressional wave slowness, and have a vertical resolution of ca. 24 inches (61.1 cm) and a depth of investigation of 12 inches (30.5 cm). Sediment porosity data were obtained from a measured density log (Fig. 2E) and core samples (Fig. 2F) (Expedition 315 Scientists 2009), and measured formation temperatures (Fig. 2G) (Expedition 315 Scientists 2009) were used to estimate thermal gradient at Site C0002. Core-derived grain density data (Expedition 315 Scientists 2009) were also used to calculate density-derived sediment porosities.

POROSITY

No core samples were obtained from depths of 200–400 m below the seafloor during Expedition 315; as such, we generated sediment porosity data using a power law regression line fitted to data obtained from drillcore data above this interval (Fig. 2F). In addition, bulk density log measurements were used to calculate sediment porosities using the standard relationship between density and porosity (Expedition 314 Scientists 2009b):

$$\phi = \frac{(\rho_m - \rho_b)}{(\rho_m - \rho_f)} \quad (1)$$

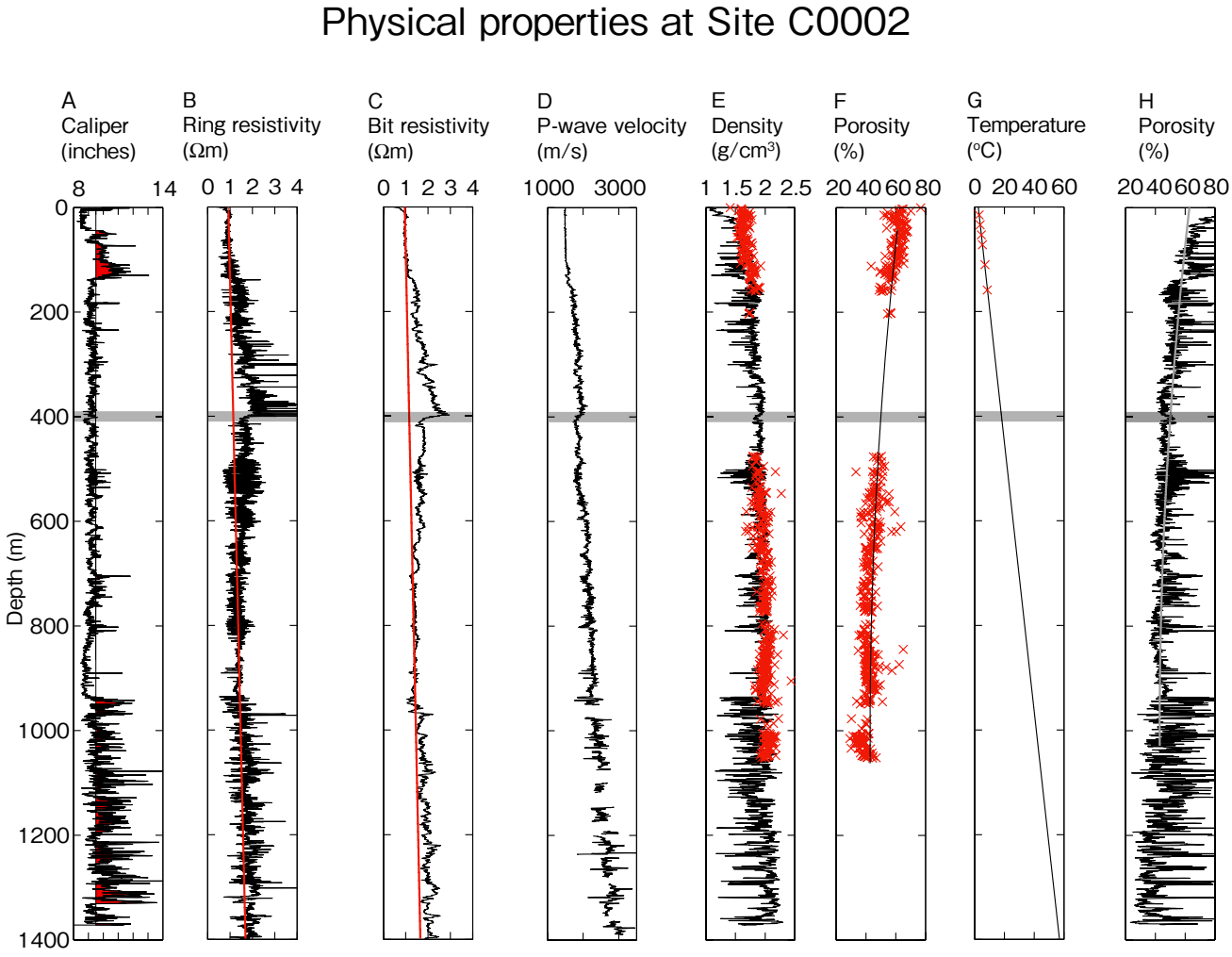

Fig. 2 Physical properties at Site C0002. (A) Caliper log from Hole C0002A (red = caliper values >9.5 inches). (B) Ring resistivity log from Hole C0002A (black line) and projected R_0 baseline (red line). (C) Bit resistivity log from Hole C0002A (black line) and projected R_0 baseline (red line). (D) P-wave velocity log from Hole C0002A. (E) Sediment densities (solid lines) from the downhole density log at Hole C0002A; crosses show core-derived wet bulk densities (red discrete points) at Holes C0002B and C0002D. (F) Core porosities (crosses) and average sediment porosities (solid lines) obtained using a power law function at Holes C0002B and C0002D. (G) Downhole temperature (crosses) at Hole C0002D with measurements fitted using a linear regression (black line). (H) Sediment porosity derived from density log data (black line) and average core sample porosities (grey line). CSF, core depth below seafloor. The depth of the BSR (400.4 m LSF) is shown by the shaded region. LSF, logging-while-drilling depth below seafloor.

Table 1 Logging units and zones at Site C0002 (Expedition 314 Scientists, 2009). LSF = LWD depth below seafloor

Depth (m LSF)	Logging unit	Zone	Interpreted lithology	Description
0–135.5	I		Unconsolidated sandy/silty mud	Basin sediments
135.5–218.1	II		Hemipelagic	
218.1–400.4		A	Hydrate-bearing zone mud and	
400.4–481.6			silty/sand	
481.6–547.1		B	Potential gas zone turbidites	
547.1–830.4				
830.4–935.6	III		Mudstone	
935.6–total depth	IV		Deformed sand/silty turbidites	Accretionary prism

where ρ_b is measured density, ρ_f is seawater density, and ρ_m is grain density. Seawater density (ρ_f) was assumed to be constant and equal to 1.024 g/cm^3 (Blum 1997). The average grain densities (ρ_m) in Units I–IV were 2.68, 2.68, 2.70, and 2.68 g/cm^3, respectively (Expedition 315 Scientists 2009).

GAS HYDRATE SATURATION

A total of eight different gas hydrate saturation calculations were used to enable the comparison of results obtained by different methods and to obtain more robust quantitative results. Two forms of the Archie equation (Archie 1942) were used to calculate gas hydrate saturation using the two types of electrical resistivity data (ring resistivity and bit resistivity) obtained during the study: the 'quick-look' Archie (Fig. 3A) and 'standard' Archie (Fig. 3B) forms. In addition, a three-phase Biot-type equation (TPE) (Leclaire *et al.* 1994; Carcione & Tinivella 2000; Lee 2007) was used to estimate gas hydrate saturation values from the Vp data (Fig. 3C). This approach of comparing gas hydrate saturation values obtained from resistivity and Vp measurements ensures that the derived saturation values are both robust and quantitatively meaningful.

The first gas hydrate saturation calculation method uses the modified 'quick-look' Archie log analysis technique (Collett & Ladd 2000). Resistivity log (R_t) measurements from Site C0002 (Fig. 2A) were used to calculate seawater saturation (S_w) values using the following modified Archie relationship:

$$S_w = \left(\frac{R_0}{R_t}\right)^{1/n} \tag{2}$$

where R_0 is the resistivity of a sedimentary section that contains seawater ($S_w = 1.0$) and n is an empirically derived constant. The parameter n depends on lithology and is typically 1.9386 (Pearson *et al.* 1983); a value of $n = 2$ was used in this study (Lee & Collett 2011). Gas hydrate and natural gas saturation (S_h) is defined as

$$S_h = 1.0 - S_w \tag{3}$$

Ring and bit resistivity data from hydrate-free parts of Units I and III were used to project R_0 trend lines (Fig. 2B,C).

The second resistivity log method is based on the 'standard' Archie equation:

$$S_w = \left(\frac{aR_w}{\phi^m R_t}\right)^{1/n} \tag{4}$$

where R_t is the resistivity of the formation obtained from logging data as either ring or bit resistivity, a is a tortuosity coefficient, R_w is the resistivity of seawater, ϕ is porosity, m is a cementation coefficient, S_w is seawater saturation, and n is the same saturation exponent used in the 'quick-look' Archie equation (Eqn 2). Values of 1.0 and 2.3 were used for a and m, respectively; these values are based on resistivity-based porosity estimates and total porosity measurements undertaken on core samples from Site C0002 (Conin *et al.* 2011). The 'standard' Archie equation was used with two different sets of sediment porosity data; the first calculation uses an average core porosity obtained from a regression line fitted to the core-derived porosity data (Fig. 2F), and the second uses sediment porosity obtained directly from the density log (Fig. 2H).

The electrical resistivity of seawater is $R_w = 1/c$, where c is the electrical conductivity of seawater that is estimated as:

$$c = 2.803 + 0.0996T \left(\Omega^{-1}\ \mathrm{m}^{-1}\right) \tag{5}$$

where T (°C) is the temperature of seawater (Shipboard Scientific Party 1995). The seawater temperature at Site C0002 was determined using a linear regression fitted to formation temperatures (Fig. 2G).

Saturation values were also estimated using Vp log data. The relationship between gas hydrate and P-wave velocities can be modeled using a TPE (Leclaire *et al.* 1994; Carcione & Tinivella 2000; Lee 2007) and by assuming that gas hydrate acts as a load-bearing component within sediments. We used a simplified TPE (Lee 2008) to calculate velocities for the gas hydrate-bearing sediments; details of the TPE used for gas hydrate-bearing sediments are given in Lee and Waite (2008) and Lee (2007, 2008). The Vp of gas hydrate-bearing sediments (Vp) was calculated as follows:

$$V_p = \sqrt{\frac{k + 4\mu/3}{\rho_b}} \tag{6}$$

where k and μ are the bulk and shear moduli of the gas hydrate-bearing sediments, respectively, and ρ_b is the bulk density of the gas hydrate-bearing sediments. The bulk density of the sediment is calculated using:

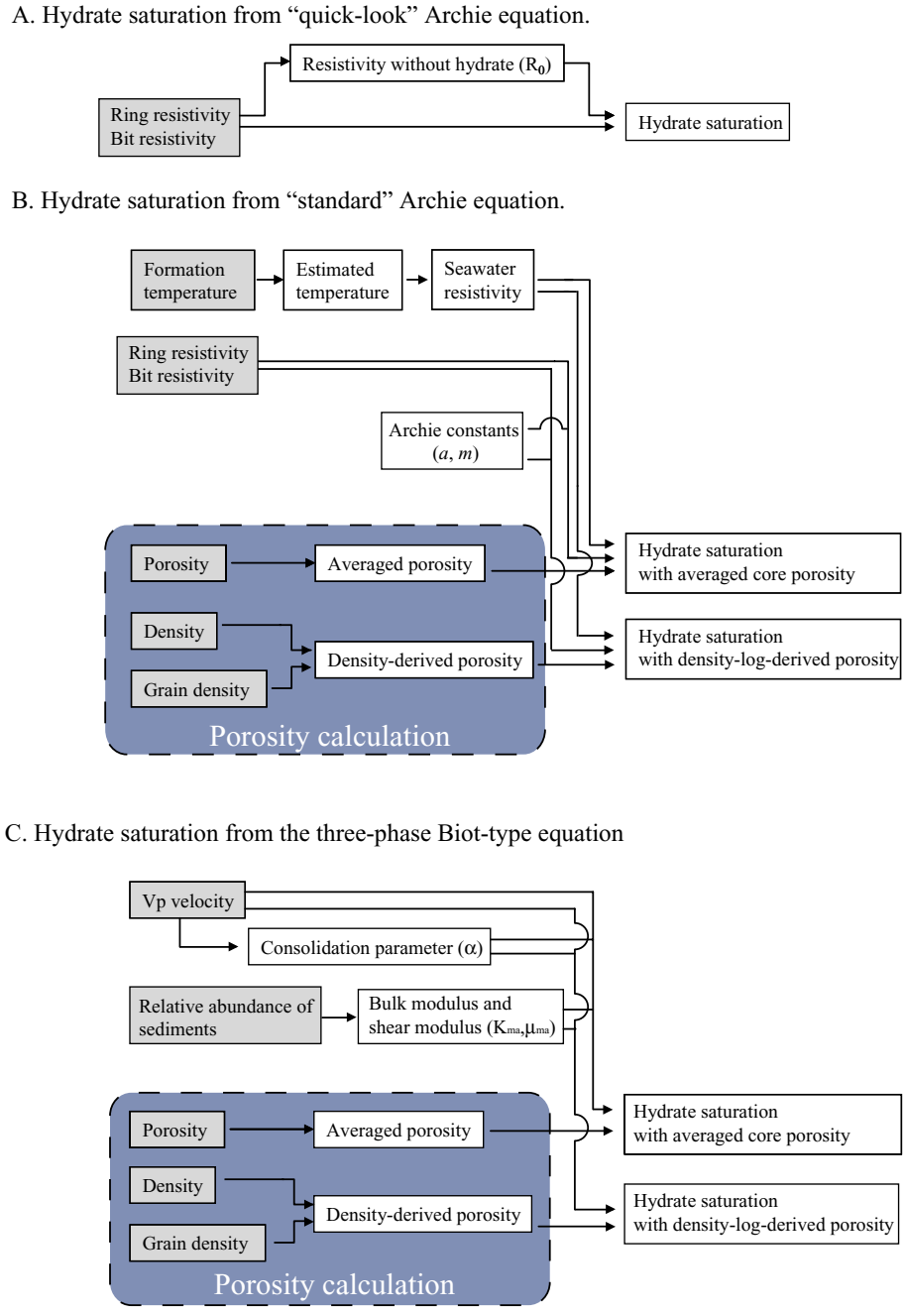

Fig. 3 Schematic illustration of flow charts for the calculations employed to estimate gas hydrate saturation values during this study. (A) 'Quick-look' Archie equation. (B) 'Standard' Archie equation. (C) Three-phase Biot-type equation. Values in the shaded boxes were measured during Expeditions 314 and 315 (Fig. 2).

$$\rho_b = \rho_{ma}(1-\phi) + \rho_w \phi (1-C_h) + \rho_h \phi C_h \qquad (7)$$

where ρ_w is the density of seawater, ρ_h is the density of pure hydrate, ρ_{ma} is the matrix density, ϕ is porosity, and C_h is the gas hydrate saturation.

The bulk and shear moduli of the gas hydrate-bearing sediments using the simplified TPE are given by Lee (2008) as, respectively:

$$k = K_{ma}(1-\beta_p) = \beta_p^2 K_{av}$$
$$\mu = \mu_{ma}(1-\beta_s) \qquad (8)$$

where

$$\frac{1}{K_{av}} = \frac{(\beta_p - \phi)}{K_{ma}} + \frac{\phi_w}{K_w} + \frac{\phi_h}{K_h},$$
$$\beta_p = \frac{\phi_{as}(1+\alpha)}{(1+\alpha\phi_{as})}, \text{ and } \beta_s = \frac{\phi_{as}(1+\gamma\alpha)}{(1+\gamma\alpha\phi_{as})}.$$

Table 2 Relative abundances of total clay minerals, quartz, plagioclase, and calcite obtained by X-ray diffraction analysis (Expedition 315 Scientists 2009) and the constants used in our modeling († = Lee 2002; ‡ = Helgerud *et al.* 1999; § = Mavko *et al.* 1998). SVD, singular value decomposition

	Water	Hydrate	Total cray	Quartz	Plagioclase	Calcite
Bulk modulus (Gpa)	2.29	6.41†	20.9‡	36.6§	75.6§	76.8§
Shear modulus (Gpa)	–	2.54†	6.85‡	45.0§	25.6§	32.0§
Abundance calculated from SVD normalization factor	–	–	47	27.8	23.2	2.1

and where ϕ_w is the porosity with water-saturated pore spaces, ϕ_h is the porosity with hydrate-saturated pore spaces, and α is a consolidation parameter (Lee 2005; Pride 2005), and:

$$\gamma = \frac{1+2\alpha}{1+\alpha} \text{ and } \phi_{as} = \phi_w + \varepsilon\phi_h. \quad (9)$$

The parameter ε accounts for the reduced impact of hydrate formation relative to compaction in terms of stiffening of the host sediment framework. Lee (2007) concluded that ε could be treated as a constant ($\varepsilon = 0.12$) when modeling the velocity of gas hydrate-bearing sediments with negligible site-to-site variability. The parameters K_{ma}, K_w, and K_h in Equation 8 are the bulk moduli of grains, seawater, and gas hydrate, respectively, and μ_{ma} is the shear moduli of the grains (Table 2); note that K_{ma} and μ_{ma} include the bulk and shear moduli of gas hydrate and are computed using the average formula of Hill (1952), provided in Helgerud *et al.* (1999). The relative abundances of total clay minerals, quartz, plagioclase, and calcite within core samples were determined using X-ray diffraction (XRD) analyses (Expedition 315 Scientists 2009), and the XRD-derived average mineral contents of gas hydrate-bearing Unit II were used to estimate K_{ma} and μ_{ma} values. The bulk and shear moduli of each material are given in Table 2 (Mavko *et al.* 1998; Helgerud *et al.* 1999; Lee 2002). We derived the values $K_{ma} = 34.5$ GPa and $\mu_{ma} = 17.1$ GPa, as estimated using the average formula of Hill (1952).

As described by Lee (2005), α is estimated to fit Vp measurements in hydrate-free zones adjacent to hydrate-bearing sands. The upper part of Unit II may contain gas hydrate, and Zone B (481.6–547.1 m LSF) has high caliper values, suggesting hole enlargement and poor log data. The deep burial below Zone B suggests that these sediments may be highly consolidated, and as such, the log data from below the BSR but above Zone B is the most suitable during use in estimating the α value. An α value of 19 was obtained by fitting Vp values between 434 and 463 m LSF, using a hydrate saturation value of zero. In addition, the TPE was used with two different sets of sediment porosity data (i.e. average core and density log porosities), as was the case for the 'standard' Archie calculation (Fig. 2H).

Any differences in the saturation values between those estimated from ring and bit resistivities and those estimated using Vp values suggest that free gas may be present. Resistivity-based gas hydrate saturation value estimates were obtained using seawater saturation values estimated from Archie's equation and Equation 3, indicating that resistivity gas hydrate saturation estimates are a combination of both hydrate and free gas. Conversely, the presence of free gas results in lower Vp values (e.g. Lee & Collett 2006) and therefore underestimates in gas hydrate saturation values derived from Vp in free-gas-bearing zones. In addition, large amounts of free gas can result in negative saturation values estimated from Vp values. This indicates that Vp-derived saturation values are lower than those obtained using resistivity data in free gas-bearing zones and, in severe cases, Vp data may yield negative apparent saturation values in zones where free gas is present. We assumed that free gas might be present where Vp-derived saturation values were both negative and were at least ca. 20% lower than saturation values estimated using resistivity data.

RESULTS

POROSITY

The average porosity of the core samples was calculated using a power law least squares approximation:

$$\phi = 2\times10^{-7}z^2 - 4\times10^{-4}z + 0.6283 \quad (10)$$

where z is depth below the seafloor. Average porosity values vary from 63% near the top of the hole to 43% at the bottom of the basin (Fig. 2F).

Density log porosity calculations for Site C0002 yielded values ranging from ca. 90% at the top of the hole to ca. 40% at the bottom of the basin (Fig. 2H). However, washouts can cause borehole enlargements, which can lead to overestimates of porosity values derived from the density log, primarily because the density logging tool considers the drilling fluid density to be the formation density. The effects of possible washouts were statistically analyzed in the interval from the upper part of Unit II to Zone A (135.5–400.4 m LSF), one of the depth zones in which we calculated gas hydrate saturation values. This approach determines correlation coefficients (r) for the relationship between borehole diameter obtained from caliper values and the density porosity using the following equation:

$$r = \frac{\sum_{i=1}^{n}(x_i - \bar{x})(y_i - \bar{y})}{\sqrt{\sum_{i=1}^{n}(x_i - \bar{x})^2 \sum_{i=1}^{n}(y_i - \bar{y})^2}} \quad (11)$$

where (x_i, y_i) is a pair of data (caliper value and porosity derived from the density log at a given depth, respectively), $\bar{x}$ and $\bar{y}$ are the arithmetic means of the caliper value and the porosity derived from the density log, respectively, and n is the number of measurements used. A positive correlation coefficient indicates that at larger hole sizes (i.e. large caliper values), density porosity values are greater, suggesting that enlargements in a hole have a significant effect on density porosity values; on the other hand, a negative correlation coefficient indicates that at larger hole sizes, density porosity values are lower, suggesting that enlargements of a hole have an insignificant effect on the density porosity. The absolute value of the correlation coefficient indicates the strength of these possible relationships. The correlation between hole size and density porosity is shown in Figure 4, and calculated correlation coefficients are given in Table 3. These correlation coefficients are positive throughout the interval from the upper part of Unit II to Zone A, with low absolute values (0.22), suggesting that a larger hole size results in an increase in the measured density porosity, although the overall effect of increases in hole size is minimal. This is supported by the fact that at depths where hole diameters are <9.5 inches, the correlation coefficient is –0.11; this negative and very low correlation coefficient suggests that any

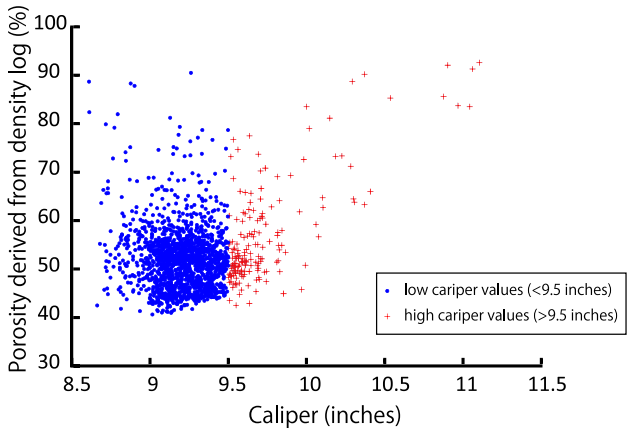

Fig. 4 Correlation diagram comparing caliper values with porosity values derived from density log data; blue dots indicate low caliper values (<9.5 inches) and red crosses indicate high caliper values (>9.5 inches).

Table 3 Calculated correlation coefficients in the interval from the upper part of Unit II to Zone A (135.5–400.4 m LSF). The correlation coefficient shown in the 'Total' column is calculated from the entire caliper dataset and the porosity derived from density log, whereas the correlation coefficient shown in the 'Low caliper values' column is calculated using porosity values and low caliper values only (<9.5 inches), and the correlation coefficient shown in the 'High caliper values' column is calculated using porosity values associated with high caliper values (>9.5 inches) only

	Total	Low caliper values (<9.5″)	High caliper values (<9.5″)
Correlation coefficient	0.22	–0.11	0.74

enlargement of the hole by washouts does not significantly affect density porosity values if the overall hole diameter is <9.5 inches. By comparison, the correlation coefficient at depths where hole sizes are >9.5 inches is 0.74; this positive and high correlation coefficient indicates that washouts that have increased hole diameters to >9.5 inches significantly affect density porosity values. Thus, data from depths at which hole diameters are >9.5 inches must be carefully assessed to see if density porosities and associated hydrate saturation estimates are accurate.

GAS HYDRATE SATURATION

Gas hydrate saturation values were estimated using the eight different approaches outlined above. Unit I is characterized by calculated apparent saturation values of <0% in all cases, probably reflecting the poor condition of the borehole

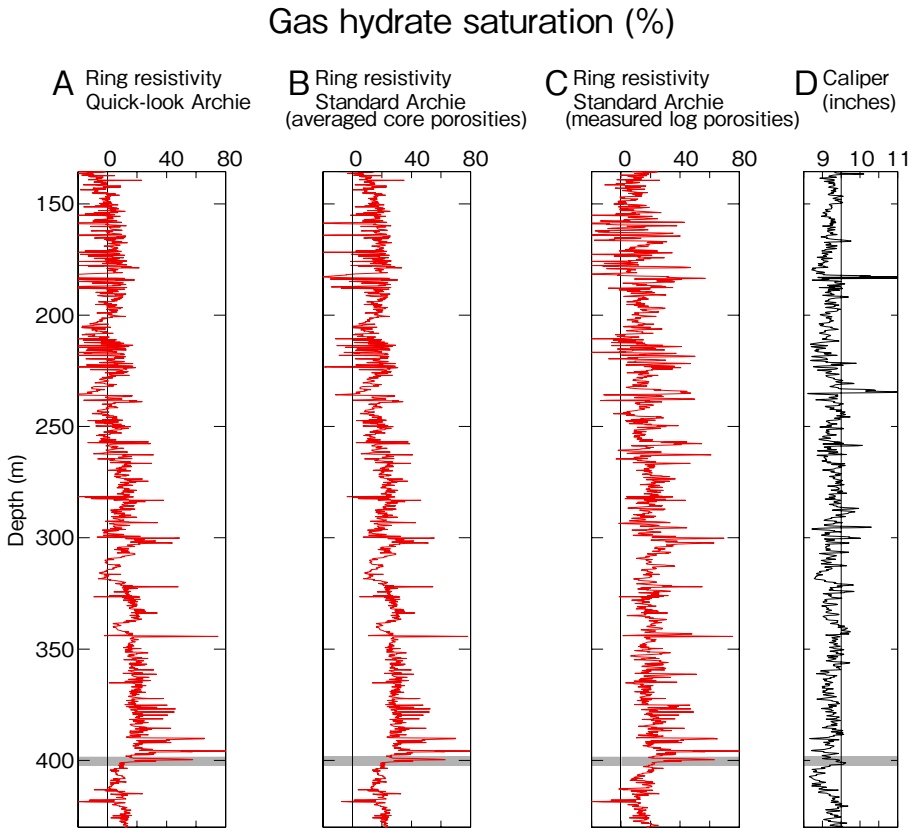

Fig. 5 Gas hydrate saturation calculated from ring resistivity log values using three different methods. (A) 'Quick-look' Archie equation. (B) 'Standard' Archie equation using average core porosity. (C) 'Standard' Archie equation using measured porosity. (D) Caliper log. The depth of the BSR (400.4 m LSF) is shown by the shaded region. LSF, logging-while-drilling depth below seafloor.

(caliper values >9.5 inches). Logging tends to underestimate the formation resistivity and Vp values of large intervals within the borehole, yielding underestimates of gas hydrate saturation values. Given this, we focused on the distribution of gas hydrate from the top of Unit II to beneath the BSR (135.5–450 m LSF) in the Kumano Basin (Figs 5–7); at these depths, caliper values are <9.5 inches, although some high-value spikes are present (Figs 5D,6D,7C). We conclude that calculated saturation values are only minimally affected by borehole washout, indicating that the saturation values obtained during this study are reliable.

Saturation calculated using ring resistivity

Gas hydrate saturation values calculated using the 'quick-look' approach and ring resistivity values vary from 0% to 10% in the shallow parts of the borehole (<258 m LSF), before gradually increasing to ca. 30% at depth below 260 m (Fig. 5A). Some saturation spikes with values of >60% are also present at depths below 280 m LSF (Fig. 5A).

Gas hydrate saturation values obtained using the 'standard' Archie equation, average core porosities, and ring resistivity values vary from 0% to 10% in the shallow parts of the borehole (<258 m LSF), before gradually increasing to ca. 35% at depth of 260 m LSF (Fig. 5B). Some saturation spikes with values of >60% are also present at depths below 280 m LSF (Fig. 5B). The 'standard' Archie equation using density log-derived porosities and ring resistivity values also yields gas hydrate saturation values of 0% to 10% at depths above 258 m LSF, increasing gradually with depth to ca. 35% (Fig. 5C). Some saturation spikes with values of >60% are evident at depths >280 m LSF; the number of spikes calculated using this approach is higher than that obtained using average core porosities (Fig. 5C), and maximum gas hydrate saturation values at these depths are ca. 80% (Fig. 5B,C).

Saturation calculated from bit resistivity

The general trend and magnitude of gas hydrate abundances estimated from bit and ring resistivity

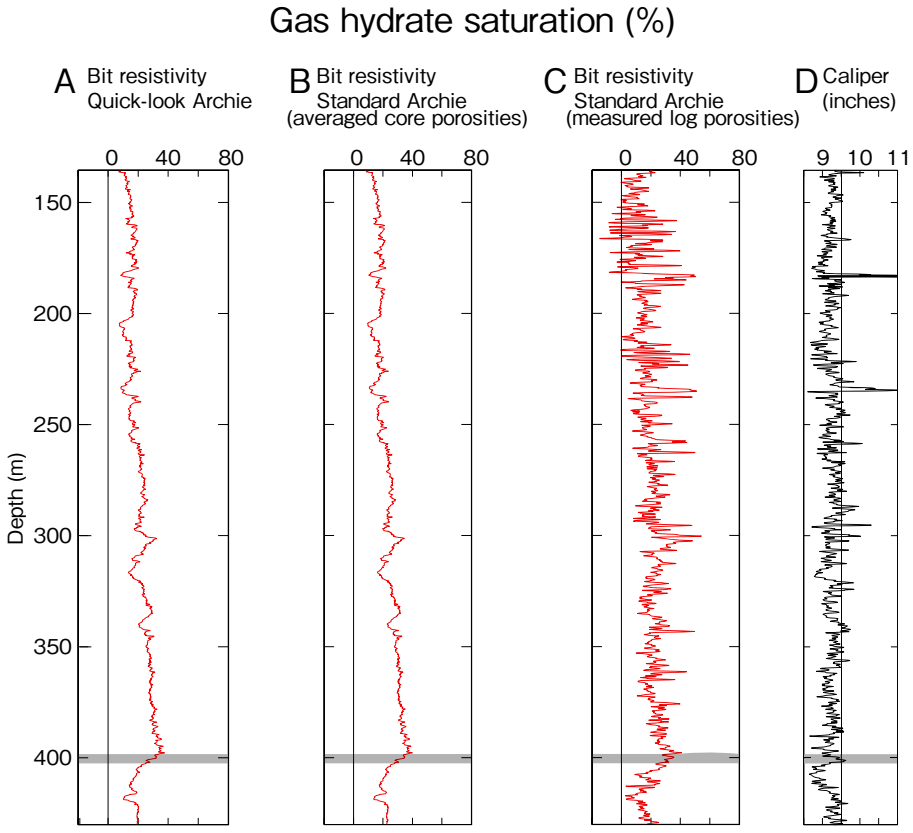

Fig. 6 Gas hydrate saturation calculated from bit resistivity log values using three different methods. (A) 'Quick-look' Archie equation. (B) 'Standard' Archie equation using average core porosity. (C) 'Standard' Archie equation using measured porosity. (D) Caliper log. The depth of the BSR (400.4 m LSF) is shown by the shaded region. LSF, logging-while-drilling depth below seafloor.

logs are similar, although changes in calculated saturation values with depth determined using bit resistivity values are relatively moderate compared with those determined using the ring resistivity log.

The gas hydrate saturation values calculated using the 'quick-look' approach and bit resistivity vary from 0% to 10% in the shallow parts of the borehole (<258 m LSF), before gradually increasing to ca. 30% at depths below 260 m LSF (Fig. 6A). By comparison, the 'standard' Archie equation combined with average core porosities and bit resistivity data yielded gas hydrate saturation values of 0% to 10% in the shallow parts of the borehole (<258 m LSF), gradually increasing with depth to ca. 35% (Fig. 6B). The 'standard' Archie equation combined with density log-derived porosities and bit resistivity data also yielded gas hydrate saturation values of 0% to 10% at depths above 258 m LSF, gradually increasing with depth to ca. 35% (Fig. 6C). Sharp saturation spikes with values of >60% observed in the ring resistivity-based saturation values are not present in the bit resistivity-derived saturation data.

Gas saturation calculated from Vp data

The gas saturation values calculated using the TPE and both average and density log porosities are very low (ca. 0%) at depths <230 m LSF (Fig. 7), but gradually increase with depth to ca. 30% (Fig. 7). The gas hydrate saturation values calculated using the TPE and density log porosities are more variable than those obtained using average porosity values.

DISCUSSION

A detailed pattern of hydrate accumulation is evident from the distribution of estimated hydrate saturation values. Calculated saturation values based on density log-derived porosities are highly variable for both the 'standard' Archie and the TPE approaches (Figs 5C,6C,7B). The use of average porosity tends to mask localized variations within complex geological systems (Collett & Ladd 2000), indicating that variations in saturation values calculated using density log porosities might reflect the detailed distribution of gas

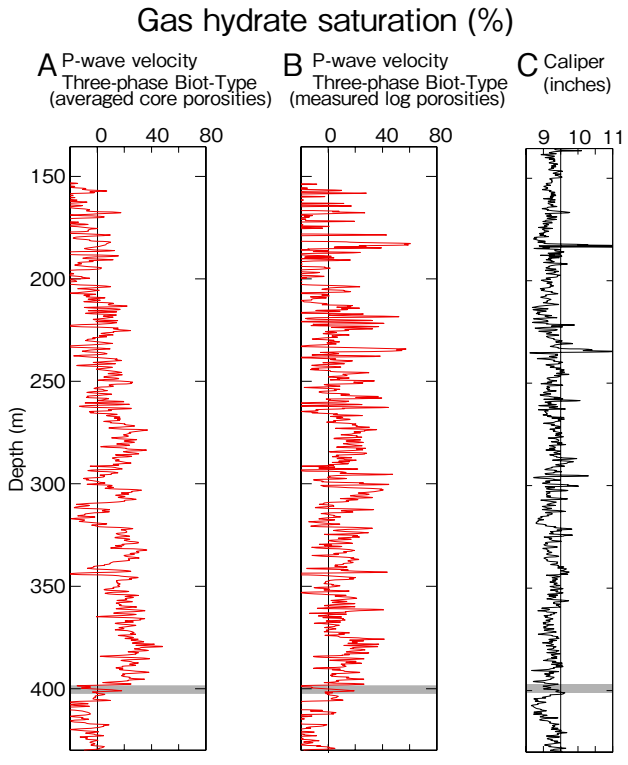

Fig. 7 Gas hydrate saturation values calculated using the Vp log and two different porosity measures. (A) A three-phase Biot-type equation using average core porosity. (B) A three-phase Biot-type equation using measured porosity. (C) Caliper log. The depth of the BSR (400.4 m LSF) is shown by the shaded band. LSF, logging-while-drilling depth below seafloor.

hydrates within the turbidite sequences encountered during drilling. The ring resistivity-derived saturation values are very high (>60%) at certain depths, a feature that is not observed in saturation values calculated using bit resistivity and Vp log data. This discrepancy may reflect differences in the vertical resolution of ring resistivity, bit resistivity, and Vp log data. The ring resistivity log has higher vertical resolution, meaning that use of these data may enable the detection of thin gas-hydrate zones within sandy layers (Saito *et al.* 2010).

Saturation values calculated using Vp data are markedly lower than those calculated from both bit and ring resistivity logs at depths just beneath the BSR (400–430 m LSF). This difference may reflect the existence of free gas in this depth interval, a finding that is consistent with results of previous studies (Expedition 314 Scientists 2009a; Saito *et al.* 2010).

The Vp- and density porosity-derived saturation values are ca. 20% lower than values obtained using bit resistivity data, and are in fact negative at several depths above 400 m LSF (e.g. 309–321 m LSF; Fig. 8). The fact that the vertical resolution and the depth of investigation is nearly the same in both the Vp and bit resistivity data means that these discrepancies are not related to differences in vertical resolutions or the depths of investigation. Moreover, the negative saturation values derived from the Vp data cannot be the result of differences in measurement methods between Vp and bit resistivity logging, and the caliper values are sufficiently small that any borehole washout effects are negligible. This suggests that these discrepancies are partly caused by the presence of free gas at these depths.

This unusual existence of free gas above the BSR can constrain the mechanisms of hydrate accumulation at Site C0002 and at the southern and seaward edge of the Kumano Basin. Free gas coexisting with gas hydrate in the gas hydrate stability zone above the BSR has been reported elsewhere (e.g. Milkov *et al.* 2004; Netzeband *et al.* 2005; Lee & Collett 2006), and Lee and Collett (2006) suggest that gas hydrates may coexist with free gas throughout the gas hydrate-bearing zone in the absence of a double BSR within the Hydrate Ridge area, offshore Oregon, USA, with free gas produced either by the dissociation of gas hydrate during drilling and/or gas transport along fractures and faults. Although dissociation of gas hydrate during drilling may have occurred at Site C0002, any dissociation is assumed to be minor as logging data were obtained with LWD immediately after drilling, and both bit resistivity and Vp measurements were undertaken deep in the formation (Expedition 314 Scientists 2009b). In addition, the bit resistivity measurement instrument was attached just above the drilling bit and the Vp measurement instrument was placed just above the former (Expedition 314 Scientists 2009b), with both measurements undertaken shortly after the drilling. Gas hydrate dissociation during drilling supposedly migrates from the borehole wall towards the interior of the formation. Even if dissociation begins immediately after drilling, it is unlikely that the dissociation migrated to the deep interior of the formation prior to the bit resistivity and Vp measurements, given the short interval between drilling and data acquisition. This indicates that the effect of gas hydrate dissociation on bit resistivity and Vp measurements is negligible. An alternative process for the formation of coexisting free gas and gas hydrate above the BSR is large fluxes of gas along fractures and faults. A high gas flux would induce rapid gas hydrate formation in the hydrate stability zone above the BSR

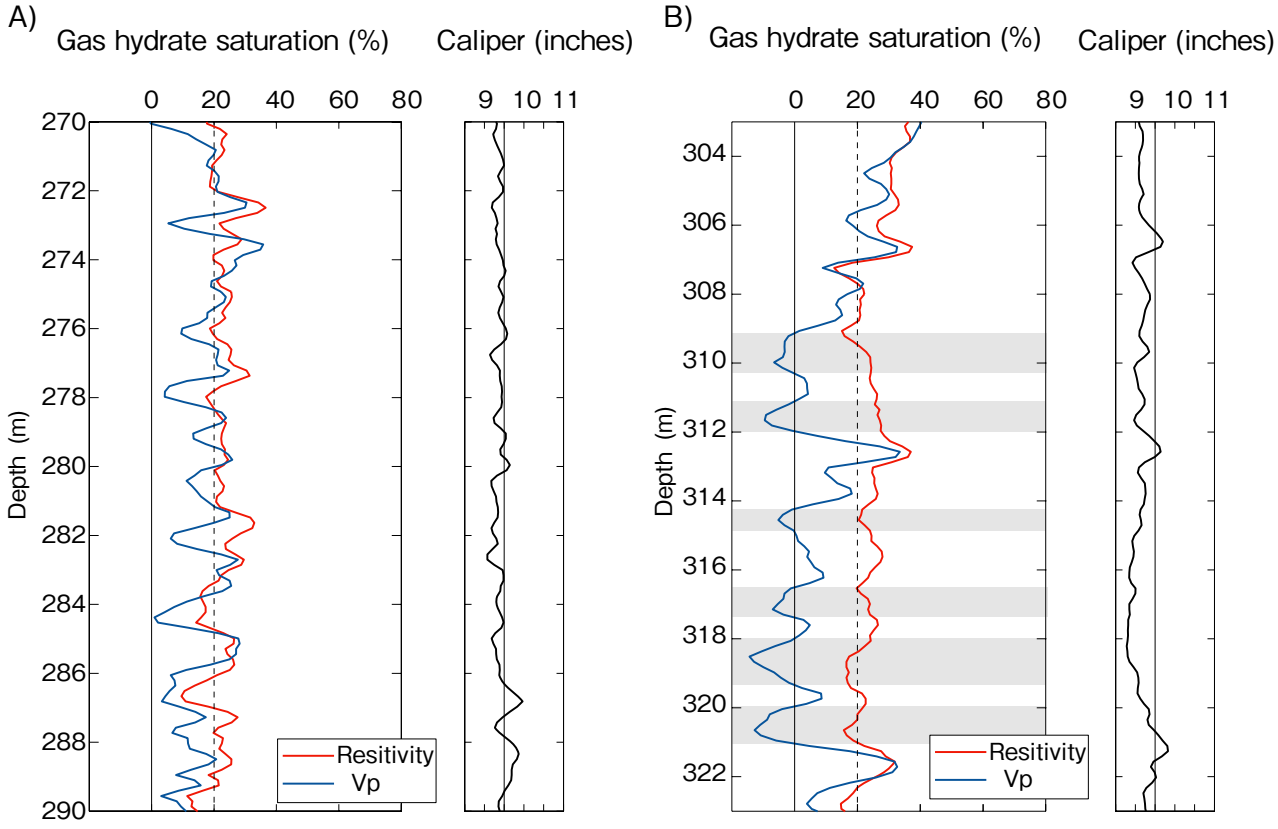

Fig. 8 Comparison of gas hydrate saturation values calculated using bit resistivity and Vp logs with density-derived porosities and caliper log values above the BSR (400 m LSF). (A) Vp-derived saturation values are very similar to resistivity log-derived saturation values. (B) Vp-derived saturation values are negative and are ca. 20% lower than values calculated using resistivity log data at the shaded depths (309–310 m, 311–312 m, 314 m, 316–317 m, 318–319 m, and 320–321 m LSF). LSF, logging-while-drilling depth below seafloor.

and lead to the coexistence of free gas and gas hydrate, primarily as a result of seawater being incorporated into gas hydrates (Suess *et al.* 1999) and/or the presence of high salinity seawater (Milkov *et al.* 2004). Doan *et al.* (2011) analyzed sonic data obtained at Site C0009, ca. 20 km northeast of Site C0002, and suggested that biogenic gas produced from organic-rich layers in the deep Kumano Basin migrates upward and accumulates within tilted layers of coarser sediments, including migrating up-dip towards the southern or seaward edge of the Kumano Basin, in the vicinity of Site C0002. A large number of landward-dipping faults (Gulick *et al.* 2010) and landward-dipping potentially high-permeability sand layers (Saito *et al.* 2010) are located in the seaward Kumano Basin. The accretionary complex that underlies the Kumano Basin may have supplied a large amount of formation fluid along thrust faults episodically (Yamada *et al.* 2014), and such deep fluids may also transport hydrocarbons. This structural setting is favorable for the transportation of large amounts of gas from the deep Kumano Basin, and suggests that the coexisting free gas and gas hydrate identified in this study may be the result of the transport of large volumes of gas from the deep and/or landward part of the Kumano Basin along fractures, faults, and high-permeability sand layers (Fig. 9).

CONCLUSIONS

Resistivity logging-derived gas hydrate saturation values at IODP Site C0002 in the Kumano Basin, Nankai Trough, Japan, range from 0% to 35%, with saturation values calculated using Vp log data ranging from 0% to 30%. Spikes in resistivity-derived saturation values (>60%) are also present and possibly indicate the presence of high concentrations of gas hydrates in thin sandy layers.

The existence of free gas in the study area is inferred from low Vp-derived saturation values beneath the BSR (400.4 m LSF). In addition, the fact that Vp-derived gas hydrate saturation values above the BSR are lower than those derived from

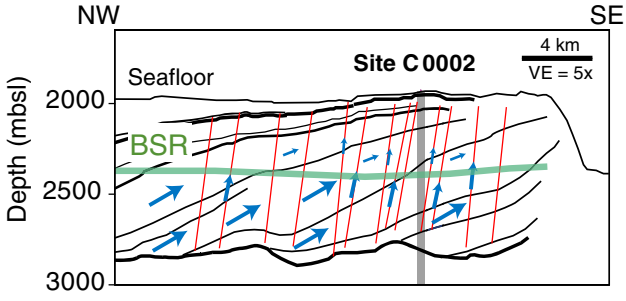

Fig. 9 Schematic illustration of free gas migration at the southern edge of the Kumano Basin in the vicinity of Site C0002. Blue arrows display free gas migration paths through NW-dipping sediments and faults; red lines indicate NW-dipping faults; the green line indicates the BSR. Most of the gas exist as gas hydrate and consequently small amount of free gas can exist (small blue arrows), though all of the gas exist as free gas (large blue arrows) below the BSR. mbsl, meters below sea level. Black lines are interpretations of the seismic profile in Figure 1 (modified after Expedition 319 Scientists 2010). VE, vertical exaggeration.

resistivity data indicates the presence of free gas. These high saturation values and the presence of free gas at site C0002 suggest that a large gas flux is taking place from deep and/or landward parts of the Kumano Basin at its southern and seaward margin.

The degree of gas hydrate saturation in the Kumano Basin at Site C0002 is ca. 30% (maximum values of ca. 80%), which is equivalent to or higher than that at other hydrate-bearing sites, such as in permafrost in Canada (Mallik 5L-38), at Mount Elbert in Alaska, in the Gulf of Mexico, within the northern Cascadia margin (Lee & Waite 2008), and in the Nankai Trough offshore from the mouth of the Tenryu River (e.g. Tsuji *et al.* 2004). These high saturation values are probably the result of the accumulation of free gas at the southern edge of the Kumano Basin; this gas was derived from elsewhere within the vast Kumano Basin and migrated along landward-dipping faults and high-permeability landward-dipping sand layers.

ACKNOWLEDGEMENTS

Samples and data were provided by the Integrated Ocean Drilling Program (IODP). We are grateful to the shipboard scientific parties and operational/technical staff of IODP Expeditions 314 and 315. This study was in part supported by the Japanese Drilling Earth Science Consortium (J-DESC), a Grant-in-Aid for Research Fellows from the Japan Society for the Promotion of Science (20-5034), and Grant-in-Aid for Scientific Research on Innovative Areas 'New perspective of Great Subduction Zone Earthquakes from Super Deep Drilling' (21107003). Prof. Toshifumi Matsuoka from Kyoto University and Dr. Yoshinori Sanada at CDEX/JAMSTEC provided comments that improved the manuscript. We also thank *Island Arc* Editor in Chief Makoto Ito, Chiba University, Dr. Tetsuya Fujii, JOGMEC and one anonymous reviewer provided constructive reviews that greatly improved the manuscript.

REFERENCES

ARCHIE G. E. 1942. The electrical resistivity log as an aid in determining some reservoir characteristics. *Journal of Petroleum Technology* **5**, 1–8.

ASHI J., TOKUYAMA H. & TAIRA A. 2002. Distribution of methane hydrate BSRs and its implication for the prism growth in the Nankai Trough. *Marine Geology* **187**, 177–91.

BABA K. & YAMADA Y. 2004. BSRs and associated reflections as an indicator of gas hydrate and free gas accumulation: An example of accretionary prism and forearc basin system along the Nankai Trough, off central Japan. *Resource Geology* **54**, 11–24.

BANGS N., HORNBACH M., MOORE G. & PARK J. 2010. Massive methane release triggered by seafloor erosion offshore southwestern Japan. *Geology* **38**, 1019–22.

BLUM P. 1997. Physical properties handbook: A guide to the shipboard measurement of physical properties of deep-sea cores. 2. Moisture and Density (by mass and volume). *ODP Technical Note* **26**, 1–15.

CARCIONE J. M. & TINIVELLA U. 2000. Bottom-simulating reflectors: Seismic velocities and AVO effects. *Geophysics* **65**, 54–67.

COLLETT T. & LADD J. 2000. Detection of gas hydrate with downhole logs and assessment of gas hydrate concentrations (saturations) and gas volumes on the Blake Ridge with electrical resistivity log data. *In* Paull C. K., Matsumot R., Wallace P. J. and Dillon W. P. (eds.) *Proceedings of the Ocean Drilling Program, Scientific Results* **164**, pp. 179–91, Ocean Drilling Program, College Station, TX.

CONIN M., HENRY P., BOURLANGE S., RAIMBOURG H. & REUSCHLÉ T. 2011. Interpretation of porosity and LWD resistivity from the Nankai accretionary wedge in light of clay physicochemical properties: Evidence for erosion and local overpressuring. *Geochemistry Geophysics Geosystems* **12**, Q0AD07. doi:10.1029/2010GC003381.

DOAN M., CONIN M., HENRY P. *et al.* 2011. Quantification of free gas in the Kumano fore-arc basin detected from borehole physical properties: IODP NanTroSEIZE drilling Site C0009. *Geochemistry Geophysics Geosystems* **12**, Q0AD06. doi:10.1029/2010GC003284.

EXPEDITION 311 SCIENTISTS 2005. Cascadia margin gas hydrates. *Integrated Ocean Drilling Program Expedition 311 Preliminary Report*. [Cited 8 March 2014.] Available from: http://publications.iodp.org/preliminary_report/311/

EXPEDITION 314 SCIENTISTS 2009a. Expedition 314, Site C0002. *In* Kinoshita M., Tobin H., Ashi J *et al.* (eds.) *Proceedings of the Integrated Ocean Drilling Program* **314/315/316**, Integrated Ocean Drilling Program Management International, Inc., Washington, DC, doi:10.2204/iodp.proc.314315316.123.2009.

EXPEDITION 314 SCIENTISTS 2009b. Expedition 314 methods. *In* Kinoshita M., Tobin H., Ashi J *et al.* (eds.) *Proceedings of the Integrated Ocean Drilling Program* **314/315/316**, Integrated Ocean Drilling Program Management International, Inc., Washington, DC, doi:10.2204/iodp.proc.314315316.123.2009.

EXPEDITION 315 SCIENTISTS 2009. Expedition 315 Site C0002. *In* Kinoshita M., Tobin H., Ashi J *et al.* (eds.) *Proceedings of the Integrated Ocean Drilling Program* **314/315/316**, Integrated Ocean Drilling Program Management International, Inc., Washington, DC, doi:10.2204/iodp.proc.314315316.124.2009.

EXPEDITION 319 SCIENTISTS 2010. Expedition 319 summary. *In* Saffer D., McNeill L., Byrne T. *et al.* (eds.) *Proceedings of the Integrated Ocean Drilling Program* **319**, Integrated Ocean Drilling Program Management International, Inc., Tokyo, doi:10.2204/iodp.proc.319.101.2010.

GULICK S., BANGS N., MOORE G. *et al.* 2010. Rapid forearc basin uplift and megasplay fault development from 3D seismic images of Nankai Margin off Kii Peninsula, Japan. *Earth and Planetary Science Letters* **300**, 55–62.

HELGERUD M., DVORKIN J., NUR A., SAKAI A. & COLLETT T. 1999. Elastic-wave velocity in marine sediments with gas hydrates: Effective medium modeling. *Geophysical Research Letters* **26**, 2021–4.

HILL R. 1952. The elastic behaviour of a crystalline aggregate. *Proceedings of the Physical Society, Section A* **65**, 349–54.

KINOSHITA M., MOORE G. F. & KIDO Y. N. 2011. Heat flow estimated from BSR and IODP borehole data: Implication of recent uplift and erosion of the imbricate thrust zone in the Nankai Trough off Kumano. *Geochemistry Geophysics Geosystems* **12**, Q0AD18. doi:10.1029/2011GC003609.

KINOSHITA M., TOBIN H., ASHI J. *et al.* 2009. NanTroSEIZE Stage 1: Investigations of seismogenesis, Nankai Trough, Japan. *Proceedings of the Integrated Ocean Drilling Program* 314/315/316, doi:10.2204/iodp.proc.314315316.2009.

KVENVOLDEN K. 1988. Methane hydrate – a major reservoir of carbon in the shallow geosphere? *Chemical Geology* **71**, 41–51.

KVENVOLDEN K. A. & MCDONALD T. J. 1985. Gas hydrates of the middle America trench – deep sea drilling project Leg 84. *Initial Reports of the Deep Sea Drilling Project* **84**, 667–82.

KVENVOLDEN K. A. & KEITH A. 1993. Gas hydrates – geological perspective and global change. *Reviews of Geophysics* **31**, 173–87.

LECLAIRE P., COHEN-TÉNOUDJI F. & AGUIRRE-PUENTE J. 1994. Extension of Biot's theory of wave propagation to frozen porous media. *The Journal of the Acoustical Society of America* **96**, 3753–68.

LEE M. 2002. Biot-Gassmann theory for velocities of gas hydrate-bearing sediments. *Geophysics* **67**, 1711–19.

LEE M. 2005. Proposed moduli of dry rock and their application to predicting elastic velocities of sandstones. *US Geological Survey Scientific Investigations Report* **2005-5119**, 1–13.

LEE M. 2007. Velocities and attenuations of gas hydrate-bearing sediments. *US Geological Survey Scientific Investigations Report* **2007-5264**, 1–11.

LEE M. 2008. Models for gas hydrate-bearing sediments inferred from hydraulic permeability and elastic velocities. *US Geological Survey Scientific Investigations Report* **2008-5219**, 1–14.

LEE M. & COLLETT T. 2011. In-situ gas hydrate saturation estimated from various well logs at the Mount Elbert Gas Hydrate Stratigraphic Test Well, Alaska North Slope. *Marine and Petroleum Geology* **28**, 439–49.

LEE M. & WAITE W. 2008. Estimating pore-space gas hydrate saturations from well log acoustic data. *Geochemistry Geophysics Geosystems* **9**, Q07008. doi:10.1029/2008GC002081.

LEE M. W. & COLLETT T. S. 2006. Gas hydrate and free gas saturations estimated from velocity logs on Hydrate Ridge, offshore Oregon, USA. *In* Tréhu A. M., Bohrmann G., Torres M. E. and Colwell F. (eds.) *Proceedings of the Ocean Drilling Program, Scientific Results* **204**, 1–25.

MAVKO G., MUKERJI T. & DVORKIN J. 1998. *The Rock Physics Handbook: Tools for Seismic Analysis in Porous Media*. Cambridge University Press, Cambridge and New York.

MILKOV A. V., DICKENS G. R., CLAYPOOL G. E. *et al.* 2004. Co-existence of gas hydrate, free gas, and brine within the regional gas hydrate stability zone at Hydrate Ridge (Oregon margin): Evidence from prolonged degassing of a pressurized core. *Earth and Planetary Science Letters* **222**, 829–43.

NETZEBAND G. L., HÜBSCHER C. P., GAJEWSKI D., GROBYS J. W. & BIALAS J. 2005. Seismic velocities from the Yaquina forearc basin off Peru: Evidence for free gas within the gas hydrate stability zone. *International Journal of Earth Sciences* **94**, 420–32.

PEARSON C. F., HALLECK P. M., MCGUIRE P. L., HERMES R. & MATHEWS M. 1983. Natural gas hydrate deposits: A review of in-situ properties. *Journal of Physical Chemistry* **87**, 4180–5.

PRIDE S. R. 2005. Relationships between seismic and hydrological properties. *In* Rubin Y. and Hubbard S. (eds.) *Hydrogeophysics*, pp. 253–90, Kluwer Academy, New York.

SAITO S., MIYAKAWA A., YAMADA Y. & KINOSHITA M. 2010. Methane hydrate occurrence estimated from downhole logging at IODP Site C0002, Kumano basin. *Journal of the Japanese Association for Petroleum Technology* **75**, 54–8.

SHIPBOARD SCIENTIFIC PARTY 1995. 4. Explanatory notes. *In* Shipley T. H., Ogawa Y., Blum P. *et al.* (eds.) *Proceedings of the Ocean Drilling Program, Initial Reports* **156**, Ocean Drilling Program, College Station, TX, doi:10.2973/odp.proc.ir.156.104.1995.

SHIPBOARD SCIENTIFIC PARTY 1997. Site 1041. *In* Kimura G., Silver E. A., Blum P. *et al.* (eds.) *Proceedings of Ocean Drilling Program, Initial Report*, **170**, pp. 153–88, Ocean Drilling Program, College Station, TX.

SUESS E., TORRES M., BOHRMANN G. *et al.* 1999. Gas hydrate destabilization: Enhanced dewatering, benthic material turnover and large methane plumes at the Cascadia convergent margin. *Earth and Planetary Science Letters* **170**, 1–15.

TAIRA A., HILL I., FIRTH J. *et al.* 1992. Sediment deformation and hydrogeology of the Nankai accretionary prism: Synthesis of shipboard results of ODP Leg 131. *Earth and Planetary Science Letters* **109**, 431–50.

TOBIN H., KINOSHITA M., ASHI J. *et al.* 2009. NanTroSEIZE stage 1 Expeditions 314, 315, and 316: First Drilling Program of the Nankai Trough Seismogezone Experiment. *Scientific Drilling* 8, 4–17.

TRÉHU A. M., BOHRMANN G., RACK F. R., TORRES M. E. *et al.* 2003. *In Proceedings of Ocean Drilling Program Initial Report*, **204**, College Station, TX. [Cited 8 March 2014.] doi:10.2973/odp.proc.ir.204.2003. Available from: http://www-odp.tamu.edu/publications/204_IR/204TOC.HTM

TSUJI Y., ISHIDA H., NAKAMIZU M., MATSUMOTO R. & SSHIMIZU S. 2004. Overview of the MITI Nankai Trough Wells: A milestone in the evaluation of methane hydrate resources. *Resource Geology* **54**, 3–10.

YAMADA Y., BABA K., MIYAKAWA A. & MATSUOKA T. 2014. Granular experiments of thrust wedges: Insights relevant to methane hydrate exploration at the Nankai accretionary prism. *Marine and Petroleum Geology* **51**, 34–48.